

# Ultrasensitive force detection with a nanotube mechanical resonator

J. Moser<sup>1,2</sup>, J. Güttinger<sup>1,2</sup>, A. Eichler<sup>1,2</sup>, M. J. Esplandiu<sup>2</sup>, D. E. Liu<sup>3</sup>, M. I. Dykman<sup>3</sup> and A. Bachtold<sup>1,2\*</sup>

**Since the advent of atomic force microscopy<sup>1</sup>, mechanical resonators have been used to study a wide variety of phenomena, including the dynamics of individual electron spins<sup>2</sup>, persistent currents in normal metal rings<sup>3</sup> and the Casimir force<sup>4,5</sup>. Key to these experiments is the ability to measure weak forces. Here, we report on force sensing experiments with a sensitivity of 12 zN Hz<sup>-1/2</sup> at a temperature of 1.2 K using a resonator made of a carbon nanotube. An ultrasensitive method based on cross-correlated electrical noise measurements, in combination with parametric downconversion, is used to detect the low-amplitude vibrations of the nanotube induced by weak forces. The force sensitivity is quantified by applying a known capacitive force. This detection method also allows us to measure the Brownian vibrations of the nanotube down to cryogenic temperatures. Force sensing with nanotube resonators offers new opportunities for detecting and manipulating individual nuclear spins as well as for magnetometry measurements.**

Force sensing with a mechanical resonator consists in converting a weak force  $F$  into a displacement  $z$  that is measurable by electrical or optical means. Advances in microfabrication in the late 1990s made it feasible to reach a force sensitivity of 820 zN Hz<sup>-1/2</sup> with ultrasoft cantilevers<sup>6,7</sup>. In spite of intensive efforts over the last decade, progress in force sensitivity has been modest. These efforts include using new materials for the resonator (such as diamond<sup>8</sup>), improving the displacement detection<sup>9,10</sup> (which can reach an imprecision below that at the standard quantum limit) and developing novel resonators (such as optically levitated nanospheres<sup>11–13</sup>). Optimizing both the resonator and its readout has led to a record sensitivity of 510 zN Hz<sup>-1/2</sup> (ref. 9).

A promising strategy for measuring lower forces is to use resonators made of a molecular system, such as a carbon nanotube<sup>14–18</sup>. Nanotube resonators are characterized by an ultralow mass  $M$ , which can be up to seven orders of magnitude lower than that of the ultrasoft cantilevers mentioned above<sup>7</sup>, whereas their quality factor  $Q$  can be high<sup>19</sup> and their spring constant  $k_0$  low. This strategy has a great potential for generating an outstanding force sensitivity, the classical limit for which is given by

$$S_F = 4k_B T \gamma = 4k_B T \sqrt{Mk_0}/Q \quad (1)$$

where  $k_B T$  is the thermal energy and  $\gamma$  the mechanical resistance<sup>7</sup>. This limit is set by the fluctuation-dissipation theorem, which associates Langevin fluctuating forces with the irreversible losses existing in a resonator, quantified by  $Q$ . Such losses may originate, for instance, from the phononic or electronic thermal bath coupled to the resonator.

Measuring the thermal vibrations (the Brownian motion) of the resonator demonstrates that its actual force sensitivity is limited by the Langevin fluctuating forces. The thermal vibrations of resonators made of single chemically synthesized nanowires have been

measured at cryogenic temperatures<sup>20</sup>. Their mass is larger than that of nanotubes, but lower than that of typical microfabricated wires. These chemically synthesized nanowires have been successfully used as force sensors<sup>20</sup>.

A challenge with resonators based on nanotubes is to detect their low-amplitude vibrations, because these vibrations are transduced into electrical and optical signals that are small and have to be extracted from an overwhelmingly large noise background. In particular, the thermal vibrations of a nanotube have not yet been detected below room temperature<sup>21</sup>. The best force sensitivity achieved thus far with nanotube resonators<sup>15,18</sup> has been limited by noise in the electrical measurement set-up, and has not surpassed the record sensitivity obtained with other resonators.

To efficiently convert weak forces into sizable displacements, we have designed nanotube resonators endowed with spring constants as low as  $\sim 10 \mu\text{N m}^{-1}$ . This is achieved by fabricating the longest possible single-walled nanotube resonators. The fabrication process starts with the growth of nanotubes by chemical vapour deposition onto a doped silicon substrate coated with silicon oxide. Using atomic force microscopy (AFM), we select nanotubes that are straight over a distance of several micrometres, so that they do not touch the underlying substrate once they are released<sup>22</sup>. We use electron-beam lithography to pattern a source and a drain electrode that electrically contact and mechanically clamp the nanotube. We suspend the nanotube using hydrofluoric acid and a critical point dryer. Figure 1a shows a 4- $\mu\text{m}$ -long nanotube resonator. We characterize its resonant frequencies by driving it electrostatically and using a mixing detection method<sup>18,23</sup>. The lowest resonant frequency is 4.2 MHz (Fig. 1c). This gives a spring constant of  $7 \mu\text{N m}^{-1}$  using an effective mass of  $1 \times 10^{-20}$  kg, estimated from the size of the nanotube measured by AFM (Supplementary Section S2.1). This spring constant is comparable to that of the softest cantilevers fabricated to date<sup>6</sup>. When changing the gate voltage  $V_g^{\text{dc}}$  applied to the silicon substrate, the resonant frequency splits into two branches (Fig. 1c). These two branches correspond to the two fundamental modes, which vibrate in directions perpendicular to one another (Fig. 1c, inset).

We have developed an ultrasensitive detection method based on parametric downconversion that (i) uses a cross-correlation measurement scheme to reduce the electrical noise in the set-up and (ii) takes advantage of the high transconductance of the nanotube in the Coulomb blockade regime to convert motion into a sizable electron current. Our detection scheme, summarized in Fig. 2a, proceeds as follows. The oscillating displacement of the nanotube, induced by the Langevin fluctuating forces, modulates the capacitance  $C_g$  between the nanotube and the gate, which in turn yields a modulation  $\delta G$  of the conductance of the nanotube. We apply a weak oscillating voltage of amplitude  $V_{\text{sd}}^{\text{ac}}$  on the source electrode at a frequency  $f_{\text{sd}}$  a few tens of kilohertz away from the resonant frequency  $f_0$ . (We verify that the amplitude of the thermal vibrations does not change upon varying  $V_{\text{sd}}^{\text{ac}}$ ,

<sup>1</sup>ICFO-Institut de Ciències Fòniques, Mediterranean Technology Park, 08860 Castelldefels (Barcelona), Spain, <sup>2</sup>ICN, CIN2-CSIC, Campus UAB, 08193 Barcelona, Spain, <sup>3</sup>Department of Physics and Astronomy, Michigan State University, East Lansing, Michigan 48824, USA. \*e-mail: adrian.bachtold@icfo.es

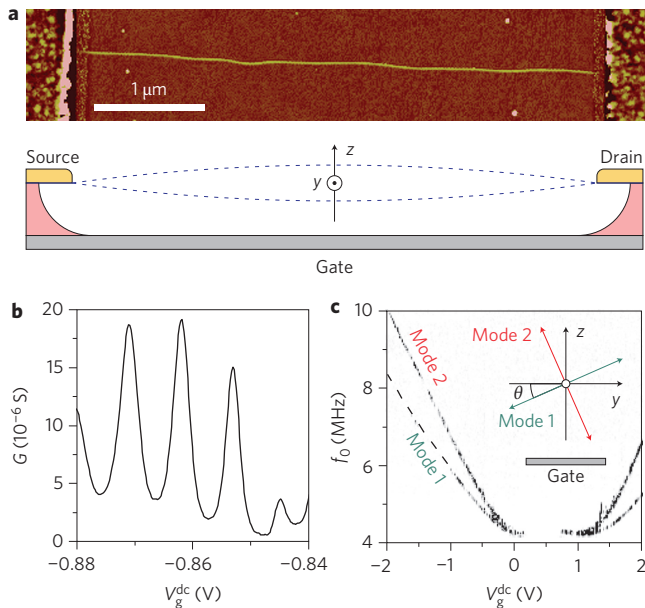


**Figure 1 | Nanotube resonator with low spring constant.** **a**, AFM image of a 4- $\mu\text{m}$ -long nanotube before removing the silicon oxide (top) and schematic of the device (bottom). **b**, Conductance  $G$  of the nanotube as a function of gate bias  $V_g^{dc}$  at 1.2 K. **c**, Resonant frequency  $f_0$  as a function of  $V_g^{dc}$  in the presence of a driving force (data obtained by measuring the mixing current with the frequency-modulation technique<sup>18,23</sup>). The two lowest frequency modes are shown. For values of  $V_g^{dc}$  ranging from  $-2$  to  $-1$  V, we indicate the resonant frequency of mode 1 with dashes because the mixing current is weak and difficult to see in the figure. The resonant frequency is highly tunable, and can change by 100% when varying  $V_g^{dc}$  by only 1.5 V. Inset: modes 1 and 2 vibrate along directions perpendicular to one another; mode 1 vibrates at an angle  $\theta$  with respect to the  $y$ -direction, which runs parallel to the gate.

Supplementary Section S2.5). The resulting current fluctuations at the drain electrode at frequency  $\sim |f_{sd} - f_0|$  are described by

$$\delta I = V_{sd}^{ac} \delta G = V_{sd}^{ac} \frac{dG}{dV_g} V_g^{dc} \frac{C_g'}{C_g} \delta z(t) \cos(2\pi f_{sd} t) \quad (2)$$

where  $dG/dV_g$  is the static transconductance of the nanotube,  $\delta z$  is the fluctuational displacement along the  $z$ -axis (Fig. 1c), and  $C_g'$  is the derivative of  $C_g$  with respect to  $z$ . To enhance  $\delta I$ , we select a nanotube that features sharp Coulomb blockade peaks (Fig. 1b), so that  $dG/dV_g$  is high for certain values of  $V_g^{dc}$ . We then convert current fluctuations into voltage fluctuations across a resistor ( $R = 2 \text{ k}\Omega$ ). This voltage signal is amplified by two independent low-noise, high-impedance amplifiers. We perform the cross-correlation of the output of the two amplifiers using a fast Fourier transform signal analyser<sup>24–26</sup>. As a result, the voltage noise of the amplifiers cancels out, and the weak signal of the thermal vibrations can be extracted from the noise background (Supplementary Section S2.3). This procedure allows us to measure the power spectral density of current fluctuations through the nanotube, which is given by  $S_I = \langle \delta I^2 \rangle / \text{rbw}$ , where  $\text{rbw}$  is the resolution bandwidth of the measurement and  $\langle \delta I^2 \rangle$  is the mean square Fourier component of the time-averaged current cross-correlation at frequency  $\sim |f_{sd} - f_0|$ . Figure 2b,c shows the resonance of the thermal vibrations at 1.2 K for the two modes characterized above, which are hereafter labelled modes 1 and 2. The lineshapes are well described by a Lorentzian function.

We observe the coupling between thermal vibrations and electrons in the Coulomb blockade regime by collecting  $S_I$  spectra as a function of  $V_g^{dc}$  for these two modes (Fig. 3a,b). The resonant

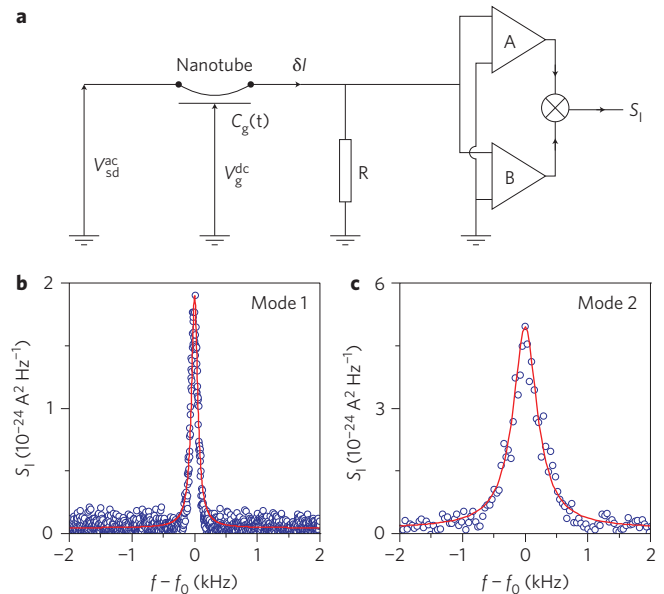


**Figure 2 | Measuring thermal vibrations.** **a**, Schematic of the cross-correlation measurement set-up. **b,c**, Power spectral density  $S_I$  of current fluctuations for modes 1 and 2 at 1.2 K, centred at the mode's resonant frequency. We apply  $V_g^{dc} = -0.854 \text{ V}$  and  $V_{sd}^{ac} = 89 \mu\text{V}$ . The mechanical quality factors are  $Q = 48,000$  for mode 1 and  $Q = 13,000$  for mode 2. We find that the quality factor of mode 2 oscillates as a function of  $V_g^{dc}$  between 8,000 and 20,000. Because the signal is weaker for mode 1, the resonance can be clearly resolved only over a limited range of  $V_g^{dc}$ .

frequency of mode 2 oscillates as a function of  $V_g^{dc}$  with the same period as the conductance oscillations (Fig. 3c), but this dependence is monotonic for mode 1. As for damping, the resonance lineshape of mode 2 is much wider than the resonance lineshape of mode 1. This is readily seen in Fig. 2b,c, where we measure  $Q = 13,000$  for mode 2 and  $Q = 48,000$  for mode 1. To understand why modes 1 and 2 exhibit distinct features, we recall that Coulomb blockade enhances the coupling between vibrations and electrons in the nanotube<sup>16,17,27</sup>, causing oscillations in resonant frequency as well as additional dissipation. The magnitude of both effects scales with the modulation of  $C_g$  induced by the nanotube vibrations, that is, with the nanotube displacement projected onto the  $z$ -direction perpendicular to the gate. The distinct behaviours measured for modes 1 and 2 indicate that mode 1 essentially vibrates parallel to the direction of the gate and mode 2 perpendicular to it (Fig. 1c, inset). Angle  $\theta$  between the vibrations of mode 1 and the direction parallel to the gate can be estimated by comparing the integrated areas of the measured spectra of modes 1 and 2, which also depend on  $C_g$ . This gives  $\theta = 19.5 \pm 2^\circ$  in the studied range of  $V_g^{dc}$  (Supplementary Section S2.4).

We then measure the force sensitivity of the resonator using a calibrating force. For this, we apply a capacitive force on mode 1 of amplitude  $F_d = C_g' V_g^{dc} V_g^{ac} \sin \theta$ , with  $V_g^{ac}(t)$  a small oscillating gate voltage at the resonant frequency of mode 1. We perform the calibration with this mode because its high  $Q$  leads to higher force sensitivity. As a result, the driven vibrations appear as a sharp peak superimposed on the thermal resonance in the  $\langle \delta I^2 \rangle$  spectrum of mode 1 (Fig. 4a). The square root of the height of this peak,  $I_{\text{peak}}$ , scales linearly with  $V_g^{ac}$ , as expected (Fig. 4b). By comparing the height of the driven peak with that of the thermal resonance using

$$S_F = \frac{\text{thermal resonance height}}{\text{driven peak height}} \times F_d^2 / \text{rbw} \quad (3)$$

we obtain  $\sqrt{S_F} = 12 \pm 8 \text{ zN Hz}^{-1/2}$  at  $T = 1.2 \text{ K}$ . Here, we use

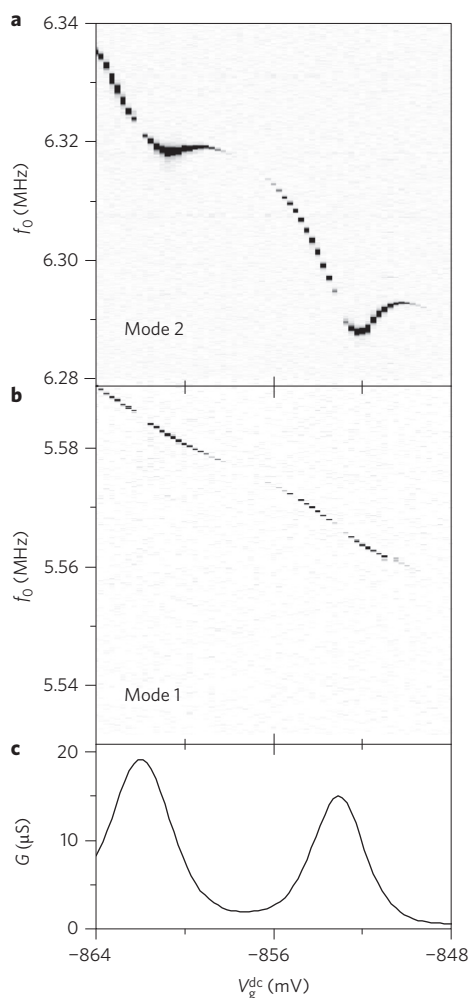


**Figure 3 | Electron-vibration coupling in the Coulomb blockade regime.** **a,b**,  $S_1$  spectra showing the resonant frequency  $f_0$  as a function of  $V_g^{dc}$  at 1.2 K for modes 1 and 2. **c**, Conductance  $G$  as a function of  $V_g^{dc}$  at 1.2 K.  $S_1$  in **a** and **b** strongly depends on  $dG/dV_g$ , as expected from equation (2).

$C_g' = 1.2(\pm 0.4) \times 10^{-12} \text{ F m}^{-1}$ , estimated from the spacing in gate voltage between the Coulomb blockade peaks and the effective distance between the nanotube and the gate. The uncertainties in  $\sqrt{S_F}$  reflect imprecisions in  $C_g'$ ,  $\theta$  and the heights of the driven peak and the thermal resonance. See Supplementary Section S1.4 for details on the measurement of the force sensitivity. Note that the voltage  $V_g^{ac}$  also induces a current of purely electrical origin (Supplementary Section S1.1), the contribution of which is negligible. This electrical contribution, which can be measured with a drive off resonance, can be detected only for exceedingly large  $V_g^{ac}$ .

We have assumed thus far that the fluctuational displacement  $\delta z$  is thermal in origin; here, we show that this assumption is correct. First, within the experimental uncertainties, the force sensitivity measured at 1.2 K is in agreement with the value expected from the fluctuation-dissipation theorem (equation (1)), which is  $23 \pm 5 \text{ zN Hz}^{-1/2}$ . The latter uncertainties reflect imprecisions in the effective mass of the nanotube (Supplementary Section S2.1) and the temperature. Second, by raising the temperature to 3 K, the measured fluctuating forces increase by an amount that agrees with the fluctuation-dissipation theorem. At 3 K, we obtain a force sensitivity of  $38 \text{ zN Hz}^{-1/2}$  (Fig. 4c,d). This is equal to the value expected at 3 K from

$$S_F(3 \text{ K}) = S_F(1.2 \text{ K}) \frac{Q(1.2 \text{ K})}{Q(3 \text{ K})} \frac{3 \text{ K}}{1.2 \text{ K}}$$

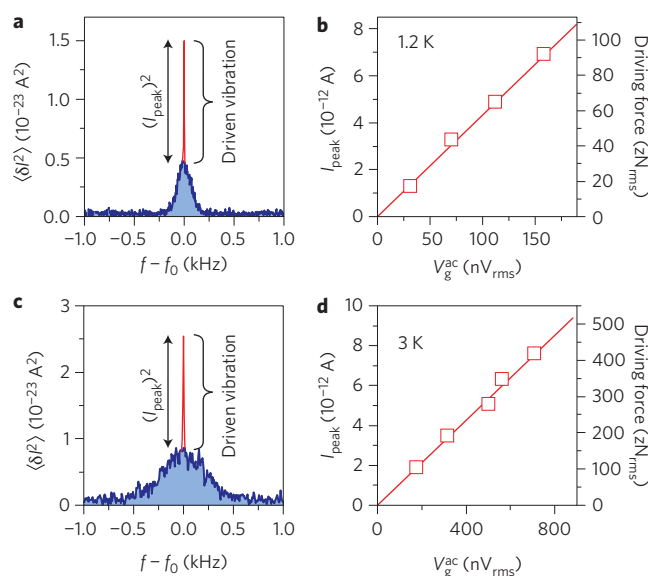


**Figure 4 | Force sensing experiment.** **a**, Square amplitude  $\langle \delta I^2 \rangle$  of the Fourier transform of the current cross-correlation at 1.2 K in the presence of a driving force at the resonant frequency of mode 1 ( $\langle \delta I^2 \rangle = S_1 \times \text{rbw}$ ). The driven vibration signal is indicated in red while the thermal vibration signal is indicated in blue. We apply  $V_{sd}^{ac} = 89 \mu\text{V}$ ,  $V_g^{dc} = -0.854 \text{ V}$  and  $V_g^{ac} = 70 \text{ nV}_{\text{rms}}$ , and set  $\text{rbw} = 4.69 \text{ Hz}$ . **b**, Square root of the driven resonance height in **a**, measured as a function of oscillating voltage  $V_g^{ac}$  applied to the gate. The straight line corresponds to a linear regression. Also shown is the driving force estimated from  $V_g^{ac}$ . **c,d**, As in **a** and **b**, but at 3 K.

according to equation (1), where we use the force sensitivity measured at 1.2 K and the quality factors extracted from the resonances at 1.2 and 3 K. Third, we estimate that non-thermal fluctuating forces do not exceed  $1 \text{ zN Hz}^{-1/2}$  at 1.2 K. Such non-thermal fluctuating forces could be the electrostatic forces induced by either the Johnson–Nyquist noise of the electrical circuit or the single-electron charging–discharging process in the Coulomb blockade regime. These two non-thermal fluctuating forces are evaluated in Supplementary Section S4. Note that the force sensitivity estimated for our nanotube resonator ( $12 \text{ zN Hz}^{-1/2}$ ) does not depend on whether the fluctuating forces are thermal or non-thermal in origin; this is because the derivation of equation (3) solely requires a fluctuating force noise that is constant over the bandwidth of the mechanical resonator.

We estimate the variance of the displacement of the thermal vibrations to be  $\sim (1.1 \text{ nm})^2$  from the equipartition theorem. We obtain a similar variance by converting the  $S_1$  spectra into displacement fluctuations. This conversion, which depends on various parameters obtained separately, is discussed in Supplementary Section S3.

Measuring the thermal vibrations of nanotube resonators sheds new light on their dynamics. Different sources of noise in nanomechanical resonators are discussed in ref. 28. Our finding that the resonance lineshape is well described by a Lorentzian function at low temperature implies that nonlinear damping is negligible<sup>18</sup>, the Duffing nonlinearity is weak, and the frequency noise is Gaussian and white<sup>29</sup>.

Carbon nanotube resonators enable an unprecedented force sensitivity on the scale of  $10 \text{ zN Hz}^{-1/2}$  at 1.2 K. We anticipate that the sensitivity will improve by at least a factor of 10 by operating the resonator at millikelvin temperatures. Indeed, the quality factor of nanotube resonators is enhanced at these temperatures<sup>19</sup>, so that both low  $T$  and high  $Q$  reduce  $S_F$ . Nanotube resonators hold promise for resonant magnetic imaging with single nuclear spin

resolution<sup>2,20,30,31</sup>. If our nanotube resonator can be integrated into the experimental set-ups described in refs 2 and 31 without degrading the force sensitivity achieved in the present work, it should be feasible to detect a single nuclear spin<sup>8</sup>. A first step in this direction will be to manipulate the nuclear spins of <sup>13</sup>C atoms naturally present in nanotubes; following ref. 20, a current-carrying wire microfabricated near the nanotube resonator could be used to generate both the magnetic field gradient and the radiofrequency magnetic field pulses (Supplementary Section S5). These resonators may also be used for ultrasensitive magnetometry measurements of individual magnetic nanoparticles and molecular magnets attached to the nanotube.

Received 22 January 2013; accepted 25 April 2013;  
published online 9 June 2013

## References

- Binnig, G., Quate, C. F. & Gerber, Ch. Atomic force microscope. *Phys. Rev. Lett.* **56**, 930–933 (1986).
- Rugar, D., Budakian, R., Mamin, H. J. & Chui, B. W. Single spin detection by magnetic resonance force microscopy. *Nature* **430**, 329–332 (2004).
- Bleszynski-Jayich, A. C. *et al.* Persistent currents in normal metal rings. *Science* **326**, 272–275 (2009).
- Mohideen, U. & Roy, A. Precision measurement of the Casimir force from 0.1 to 0.9  $\mu\text{m}$ . *Phys. Rev. Lett.* **81**, 4549–4552 (1998).
- Chan, H. B., Aksyuk, V. A., Kleiman, R. N., Bishop, D. J. & Capasso, F. Quantum mechanical actuation of microelectromechanical systems by the Casimir force. *Science* **291**, 1941–1944 (2001).
- Stowe, T. D. *et al.* Attonewton force detection using ultrathin silicon cantilevers. *Appl. Phys. Lett.* **71**, 288–290 (1997).
- Mamin, H. J. & Rugar, D. Sub-attonewton force detection at millikelvin temperatures. *Appl. Phys. Lett.* **79**, 3358–3360 (2001).
- Tao, Y., Boss, J. M., Moores, B. A. & Degen, C. L. Single-crystal diamond nanomechanical resonators with quality factors exceeding one million. Preprint at <http://xxx.lanl.gov/abs/1212.1347> (2012).
- Teufel, J. D., Donner, T., Castellanos-Beltran, M. A., Harlow, J. W. & Lehnert, K. W. Nanomechanical motion measured with an imprecision below that at the standard quantum limit. *Appl. Phys. Lett.* **102**, 151910 (2013).
- Gavartin, E., Verlot, P. & Kippenberg, T. J. A hybrid on-chip optomechanical transducer for ultrasensitive force measurements. *Nature Nanotech.* **7**, 509–514 (2012).
- Chang, D. E. *et al.* Cavity opto-mechanics using an optically levitated nanosphere. *Proc. Natl Acad. Sci. USA* **107**, 1005–1010 (2009).
- Li, T., Kheifets, S. & Raizen, M. G. Millikelvin cooling of an optically trapped microsphere in vacuum. *Nature Phys.* **7**, 527–530 (2011).
- Gieseler, J., Deutsch, B., Quidant, R. & Novotny, L. Subkelvin parametric feedback cooling of a laser-trapped nanoparticle. *Phys. Rev. Lett.* **109**, 103603 (2012).
- Reulet, B. *et al.* Acoustoelectric effects in carbon nanotubes. *Phys. Rev. Lett.* **85**, 2829–2832 (2000).
- Sazonova, V. *et al.* A tunable carbon nanotube electromechanical oscillator. *Nature* **431**, 284–287 (2004).
- Lassagne, B., Tarakanov, Y., Kinaret, J., Garcia-Sanchez, D. & Bachtold, A. Coupling mechanics to charge transport in carbon nanotube mechanical resonators. *Science* **325**, 1107–1110 (2009).
- Steele, G. A. *et al.* Strong coupling between single-electron tunneling and nanomechanical motion. *Science* **325**, 1103–1107 (2009).
- Eichler, A., Moser, J., Chaste, J., Zdrojek, M., Wilson-Rae, I. & Bachtold, A. Nonlinear damping in mechanical resonators made from carbon nanotubes and graphene. *Nature Nanotech.* **6**, 339–342 (2011).
- Hüttel, A. K. *et al.* Carbon nanotubes as ultrahigh quality factor mechanical resonators. *Nano Lett.* **9**, 2547–2552 (2009).
- Nichol, J. M., Hemesath, E. R., Lauthon, L. J. & Budakian, R. Nanomechanical detection of nuclear magnetic resonance using a silicon nanowire oscillator. *Phys. Rev. B* **85**, 054414 (2012).
- Stapfner, S. *et al.* Cavity-enhanced optical detection of carbon nanotube Brownian motion. *Appl. Phys. Lett.* **102**, 151910 (2013).
- Chaste, J., Slezinska, M., Zdrojek, M., Moser, J. & Bachtold, A. High-frequency nanotube mechanical resonators. *Appl. Phys. Lett.* **99**, 213502 (2011).
- Gouttenoire, V. *et al.* Digital and FM demodulation of a doubly clamped single-walled carbon-nanotube oscillator: towards a nanotube cell phone. *Small* **6**, 1060–1065 (2010).
- Glatli, D. C., Jacques, P., Kumar, A., Pari, P. & Saminadayar, L. A noise detection scheme with 10 mK noise temperature resolution for semiconductor single electron tunneling devices. *J. Appl. Phys.* **81**, 7350–7356 (1997).
- Saminadayar, L., Glatli, D. C., Jin, Y. & Etienne, B. Observation of the  $e/3$  fractionally charged Laughlin quasiparticle. *Phys. Rev. Lett.* **79**, 2526–2529 (1997).
- Henny, M., Oberholzer, S., Strunk, C. & Schönberger, C.  $1/3$ -shot-noise suppression in diffusive nanowires. *Phys. Rev. B* **59**, 2871–2880 (1999).
- Ganzhorn, M. & Wernsdorfer, W. Dynamics and dissipation induced by single-electron tunneling in carbon nanotube nanoelectromechanical systems. *Phys. Rev. Lett.* **108**, 175502 (2012).
- Cleland, A. N. & Roukes, M. L. M. Noise processes in nanomechanical resonators. *J. Appl. Phys.* **92**, 2758–2769 (2002).
- Maizelis, Z. A., Roukes, M. L. & Dykman, M. I. Detecting and characterizing frequency fluctuations of vibrational modes. *Phys. Rev. B* **84**, 144301 (2011).
- Poggio, M. & Degen, C. L. Force-detected nuclear magnetic resonance: recent advances and future challenges. *Nanotechnology* **21**, 342001 (2010).
- Degen, C. L., Poggio, M., Mamin, H. J., Rettner, C. T. & Rugar, D. Nanoscale magnetic resonance imaging. *Proc. Natl Acad. Sci. USA* **106**, 1313–1317 (2009).

## Acknowledgements

The authors thank C. Degen, C. Glatli, C. Schönberger, J. Gabelli and T. Kontos for discussions. We acknowledge support from the European Union through the RODIN-FP7 project, the ERC-carbonNEMS project and a Marie Curie grant (271938), the Spanish state (FIS2009-11284), the Catalan government (AGAUR, SGR) and the US Army Research Office.

## Author contributions

J.M. fabricated the device, developed the experimental set-up, and carried out the measurements. J.G. and A.E. provided support with the experimental set-up. J.G. participated in the measurements. J.G. and J.M. analysed the data. M.J.E. grew the nanotubes. D.E.L. and M.I.D. provided support with the theory and wrote the theoretical part of the Supplementary Information. J.M. and A.B. wrote the manuscript with critical comments from J.G. and M.I.D. A.B. conceived the experiment and supervised the work.

## Additional information

Supplementary information is available in the online version of the paper. Reprints and permissions information is available online at [www.nature.com/reprints](http://www.nature.com/reprints). Correspondence and requests for materials should be addressed to A.B.

## Competing financial interests

The authors declare no competing financial interests.